Efficient Transmitter Selection Strategies for Improved Information Gathering of Aerial Vehicle Navigation in GNSS-Denied Environments

Alexander A. Nguyen and Zaher M. Kassas, *Senior Member, IEEE*

***Abstract*—Aerial vehicle navigation in global navigation satellite system (GNSS)-denied environments by utilizing pseudorange measurements from M terrestrial signals of opportunity (SOPs) is considered. To this end, the aerial vehicle is tasked with choosing $K < M$ most informative terrestrial SOPs. Two computationally efficient, but sub-optimal, transmitter selection strategies are proposed. These selection strategies, termed opportunistic greedy selection (OGS) and one-shot selection (OSS), exploit the additive, iterative properties of the Fisher information matrix (FIM), where OGS selects the most informative transmitters in finite iterations, while the OSS selects in one-iteration. Monte Carlo simulation results are presented comparing the OGS and OSS strategies versus the optimal (exhaustive search) selection strategy, where it is concluded that OGS performs closely to the optimal selection, while executing in a fraction of the optimal selection's time. Experimental results are presented of a U.S. Air Force high-altitude aircraft navigating without GNSS signals in (i) a rural region and (ii) a semi-urban region. The performance of the aircraft's navigation solution with the selected SOP transmitters via optimal, OGS, OSS are compared over a flight segment where the selection remained valid. The position root mean-squared error (RMSE) with the optimal, OGS, and OSS were 4.53 m, 6.28 m, 7.13 m in the rural region; and 5.83 m, 6.08 m, 6.70 m in the semi-urban region for an aircraft traversing a trajectory of 1.48 km and 1.22 km, respectively.**

***Index Terms*—Signals of opportunity, aerial vehicle navigation, sensor selection**

I. Introduction

Modern aerial vehicle navigation systems, whether low-altitude unmanned aerial vehicles (UAVs) or high-altitude aircraft, rely on global navigation satellite system (GNSS) signals [1]. However, relying on GNSS alone does not yield a continuous flow of resilient position, velocity, and time estimates. In recent years, GNSS radio frequency interference (RFI) incidents have increased dramatically, threatening the safety of flight operations [2], calling for a reliable alternative to GNSS signals in the event that these signals become unusable [3]. Signals of opportunity (SOPs) [4]–[7] have been the subject of extensive research, where they have shown promise to be a standalone navigation alternative to GNSS. SOPs can be terrestrial-based (e.g., FM radio [8], [9], cellular [10]–[13], and digital television [14], [15]) or space-based (e.g., low Earth orbit (LEO) satellites [16]–[18]). Among terrestrial SOPs, cellular signals have shown the most promise for aerial vehicle navigation [19], achieving submeter-level accuracy in a standalone [20] and differential [21] navigation fashion.

Assessing terrestrial SOPs on low-altitude UAVs and high-altitude aircraft has been considered in the context of channel modeling, communication, and navigation [22]–[25]. Of particular note is the recent week-long flight campaign by the Autonomous Systems Perception, Intelligence, and Navigation (ASPIN) Laboratory in collaboration with the United States Air Force (USAF) to study the potential of cellular SOPs for high-altitude aircraft navigation. This campaign, called "SNIFFER: Signals of opportunity for Navigation In Frequency-Forbidden EnviRonments," revealed that terrestrial cellular SOPs can be acquired and tracked at altitudes reaching 23,000 ft above ground level and at horizontal distances of more than 100 km away, and could yield meter-level accurate navigation solutions without GNSS [26], [27].

At high altitudes, it was recently discovered that more than a hundred cellular SOPs can be acquired and tracked, from which pseudorange measurements can be extracted [28]. Tracking all such SOPs simultaneously could be formidable on platforms with limited size, weight, power, and cost (SWaP-C) or unnecessary, since tracking a subset of the SOPs could yield a comparable performance. As such this article considers the transmitter selection problem, where an aerial vehicle is tasked with selecting a subset of the SOPs, to minimize the receiver's computational strain. Fig. 1 illustrates a real-world scenario in which the problem of transmitter selection was encountered. Here, the white pins denote $M = 57$ cellular SOPs which the aerial vehicle-mounted receiver was able to acquire and track.

A similar problem to transmitter selection has been studied in the literature in the context of sensor selection for target tracking [29], [30]. Sensor selection problems are typically formulated as an integer programming (IP) problem, which is difficult to solve in a computationally efficient fashion, while finding the optimal solution via exhaustive search becomes formidable for large sensor networks. To circumvent this, several heuristic and sub-optimal algorithms have been proposed.

This work was supported in part by the National Science Foundation (NSF) Grant 1929571 and in part by the Air Force Office of Scientific Research (AFOSR) under Grant FA9550-22-1-0476. This work was also supported in part by the Laboratory Directed Research and Development program at Sandia National Laboratories, a multimission laboratory managed and operated by National Technology and Engineering Solutions of Sandia LLC, a wholly owned subsidiary of Honeywell International Inc. for the U.S. Department of Energy's National Nuclear Security Administration under contract DE-NA0003525. This paper describes objective technical results and analysis. Any subjective views or opinions that might be expressed in the paper do not necessarily represent the views of the U.S. Department of Energy or the United States Government. SAND2022-13901 C

A. Nguyen is with the Department of Mechanical and Aerospace Engineering, University of California, Irvine. Z. Kassas is with the Department of Electrical and Computer Engineering, The Ohio State University. (*Corresponding author: Z. Kassas*, email: zkassas@ieee.org).

Some approaches formulate the sensor selection problem as a convex or non-convex optimization problem [31]–[35]. Others have approached this problem as a greedy sensor selection by leveraging the notion of submodularity [36], [37] or by utilizing the Fisher information matrix (FIM) [38], [39].

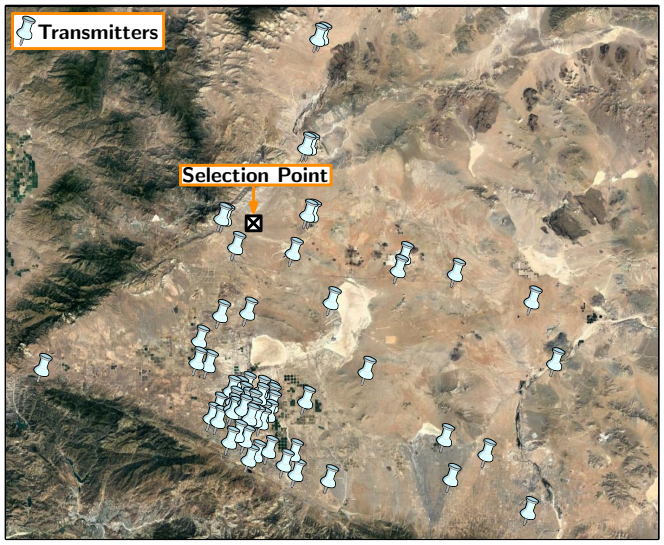

Fig. 1. Motivating example. $M = 57$ terrestrial SOP transmitters (white) in the environment relative to the aerial vehicle's selection point (black cross). What is the "best" (most informative) $K < M$ subset of SOPs for navigation?

It is rather difficult to explicitly solve the transmitter selection optimization problem efficiently for a large number of transmitters due to the integer constraints. As such, this article aims to extend the findings in [40] by proposing two sub-optimal, computationally efficient transmitter selection strategies, termed opportunistic greedy selection (OGS) and one-shot selection (OSS). The proposed strategies are simple, yet highly-effective at selecting the "best" transmitters without explicitly solving the IP problem. The proposed strategies exploit the additive, iterative properties of the FIM, where the OGS selects the most informative transmitters in finite iterations (i.e., recursively), while the OSS selects in one iteration (i.e., batch). Numerical simulations are presented analyzing the performance of the proposed selection strategies, where it is concluded that OGS performs closely to the optimal selection, while executing in a fraction of the optimal selection's time. Experimental results are also presented for a USAF high-altitude aircraft navigating without GNSS in a rural and a semi-urban region. The effectiveness of the selected SOPs on the navigation performance is also demonstrated. The position root mean-squared error (RMSE) with the optimal, OGS, and OSS were 4.53 m, 6.28 m, 7.13 m in the rural region; and 5.83 m, 6.08 m, 6.70 m in the semi-urban region for an aircraft traversing a trajectory of 1.48 km and 1.22 km, respectively. It is important to highlight that the SOP selection subset was found to be valid over a trajectory of several kilometers, since the aerial vehicle-to-SOP geometry is approximately stationary for sufficiently faraway SOPs.

The remainder of this article is organized as follows. Section II overviews the considered problem. Section III formulates the transmitter selection problem. Section IV presents the selection strategies. Section V analyzes the proposed selection strategies. Section VI presents simulation results. Section VII presents experimental results for an aerial vehicle flying in two different regions. Section VIII gives concluding remarks.

II. Problem Description

To motivate the transmitter selection problem, consider the scenario depicted in Fig. 2, in which an aerial vehicle is navigating in an environment comprising M terrestrial SOP transmitters. During flight, the aerial vehicle experiences GNSS outage (e.g., due to RFI or spoofing). The aerial vehicle is assumed to have a map of the SOP locations (e.g., loaded prior to flight or transmitted from a nearby uplink station). The aerial vehicle is assumed to be equipped with receivers capable of extracting pseudorange measurements from the SOPs, which will be used instead of GNSS to navigate the aerial vehicle. Due to SWaP-C constraints (e.g., limited payload, processing power, etc.), the aerial vehicle can only use signals from ($K < M$) SOPs. What is the "best" (most informative) SOP subset to select?

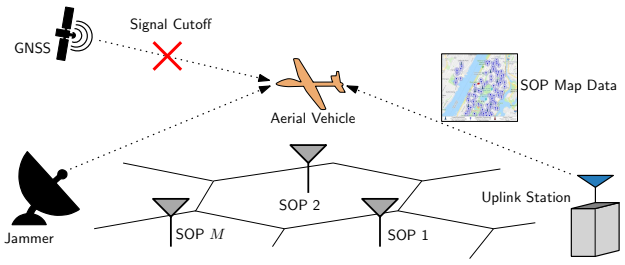

Fig. 2. Problem description. An aerial vehicle is equipped with a receiver capable of extracting pseudorange measurements from terrestrial SOPs. During flight, the aerial vehicle experiences GNSS outage. A nearby uplink station sends SOP map data to the aerial vehicle, which contains the locations of M terrestrial SOPs. The aerial vehicle's selects the "best" (most informative) $K < M$ to use to continue navigating.

III. Problem Formulation

This section formulates the transmitter selection problem.

A. Pseudorange Measurement Model

Consider an aerial vehicle equipped with an onboard receiver capable of extracting pseudorange measurements from M terrestrial SOPs in the environment. The pseudorange measurement made by the receiver to the i^{th} SOP, after discretization and mild approximations, is modeled as

$$z_{s_i}(k) = \underbrace{\left\|\boldsymbol{r}_r(k) - \boldsymbol{r}_{s_i}\right\|_2 + c \cdot [\delta t_r(k) - \delta t_{s_i}(k)]}_{h_i[\boldsymbol{x}(k)]} + v_{s_i}(k), \tag{1}$$

where $\boldsymbol{r}_r = [x_r,\ y_r, z_r]^{\mathsf{T}}$ is the three-dimensional (3–D) position vector of the aerial vehicle, $\boldsymbol{r}_{s_i} = [x_{s_i},\ y_{s_i}, z_{s_i}]^{\mathsf{T}}$ is the 3–D position vector of the i^{th} SOP, δt_r is the aerial vehicle-mounted receiver's clock bias, δt_{s_i} is the i^{th} SOP's clock bias, c is the speed of light, and v_{s_i} is the i^{th} SOP's measurement noise, which is modeled as a zero-mean white Gaussian sequence with variance $\sigma^2_{s_i}$ and is assumed to be independent across all SOPs. The dynamics of the clock error is described in Appendix A.

B. Fisher Information Matrix

The proposed transmitter selection strategies aim to choose the most informative measurements, which motivates adopting the FIM defined as

$$\mathbf{I}(\boldsymbol{x}) = \mathbb{E}\left[\left(\frac{\partial \ln\, p(\boldsymbol{z}|\boldsymbol{x})}{\partial \boldsymbol{x}}\right)\left(\frac{\partial \ln\, p(\boldsymbol{z}|\boldsymbol{x})}{\partial \boldsymbol{x}}\right)^{\mathsf{T}}\right]$$

where $p(\boldsymbol{z}|\boldsymbol{x})$ is the likelihood function of the measurements $\boldsymbol{z}$ parameterized by the states $\boldsymbol{x}$. Since the noise in the measurement model (1) is assumed to be independent across all SOPs, the FIM can be written as the prior FIM plus a summation of the information content associated with each measurement, i.e.,

$$\begin{aligned}\mathbf{I}(\boldsymbol{x}) &= \mathbf{I}_0(\boldsymbol{x}) + \sum_{i=1}^{M} \frac{1}{\sigma_{s_i}^2}\left(\frac{\partial h_i(\boldsymbol{x})}{\partial \boldsymbol{x}}\right)\left(\frac{\partial h_i(\boldsymbol{x})}{\partial \boldsymbol{x}}\right)^{\mathsf{T}} \quad (2)\\ &= \mathbf{I}_0(\boldsymbol{x}) + \sum_{i=1}^{M} \mathbf{I}_i(\boldsymbol{x}),\end{aligned}$$

The additive property of information from different sources [41] will be utilized in the proposed transmitter selection strategies. Denoting the (prior) information content associated with a subset of SOPs as $\mathbf{I}_0(\boldsymbol{x})$ and the information associated with the i^{th} SOP as $\mathbf{I}_i(\boldsymbol{x})$, the (posterior) information content associated with updating the SOP subset to include the i^{th} SOP is defined as $\mathbf{I}_{\text{posterior},i}(\boldsymbol{x}) = \mathbf{I}_0(\boldsymbol{x}) + \mathbf{I}_i(\boldsymbol{x})$. Appendix B relates the FIM to the horizontal dilution of precision (HDOP) metric, commonly used in positioning and navigation.

C. Estimation Framework

Generally, one needs to estimate the state vector $\boldsymbol{x}$, which includes the aerial vehicle's position $\boldsymbol{r}_r$ and velocity $\dot{\boldsymbol{r}}_r$ as well as relative clock error states $\{\boldsymbol{x}_{\text{clk},i}\}_{i=1}^{M}$ between the vehicle-mounted receiver and each SOP, namely

$$\boldsymbol{x} \triangleq \left[\boldsymbol{r}_r^{\mathsf{T}},\ \dot{\boldsymbol{r}}_r^{\mathsf{T}},\ \boldsymbol{\Delta x}_{\text{clk},1}^{\mathsf{T}},\ \ldots,\ \boldsymbol{\Delta x}_{\text{clk},M}^{\mathsf{T}}\right]^{\mathsf{T}},$$

$$\boldsymbol{\Delta x}_{\text{clk},i} \triangleq \left[c\cdot(\delta t_r - \delta t_{s_i}),\, c\cdot(\dot{\delta} t_r - \dot{\delta} t_{s_i})\right]^{\mathsf{T}}.$$

Formulating the transmitter selection problem with $\boldsymbol{x} \in \mathbb{R}^{6+2M}$ results in a large-scale optimization problem. To scale down the problem, two simplifications are made. First, it is noted that terrestrial SOPs suffer from poor geometric diversity in the vertical direction (particular as seen by high-altitude aircraft). Therefore, relying exclusively on SOPs for 3–D navigation leads to a large vertical dilution of precision (VDOP) [42], [43]. Hence, it is assumed that the aerial vehicle is equipped with an altimeter to determine its altitude. As such, in what follows, the problem is formulated to only consider the 2–D (planar) aerial vehicle states. Second, only the position states of the aerial vehicle will be considered, leading to the redefined state vector $\boldsymbol{x}' \in \mathbb{R}^2$. It will be demonstrated in Subsection VI-B that this simplification, which ignores the timing states, results in a negligible increase in position uncertainty (on the order of sub-meter).

A static, weighted nonlinear least-squares (WNLS) estimator is employed on the redefined state vector $\boldsymbol{x}'$. The resulting Jacobian matrix $\mathbf{H}_r$ is given by

$$\mathbf{H}_{\boldsymbol{r}_r} = \begin{bmatrix} \frac{\boldsymbol{r}_r^{\mathsf{T}} - \boldsymbol{r}_{s_1}^{\mathsf{T}}}{\|\boldsymbol{r}_r - \boldsymbol{r}_{s_1}\|_2} \\ \vdots \\ \frac{\boldsymbol{r}_r^{\mathsf{T}} - \boldsymbol{r}_{s_M}^{\mathsf{T}}}{\|\boldsymbol{r}_r - \boldsymbol{r}_{s_M}\|_2} \end{bmatrix}. \quad (3)$$

The WNLS estimation error covariance matrix is given by

$$\mathbf{P}_{\boldsymbol{r}_r} \triangleq \left[\mathbf{P}_{0,\boldsymbol{r}_r}^{-1} + \mathbf{H}_{\boldsymbol{r}_r}^{\mathsf{T}}\mathbf{R}^{-1}\mathbf{H}_{\boldsymbol{r}_r}\right]^{-1}, \quad (4)$$

where a prior of $\boldsymbol{x}'$ may be given, denoted by $\hat{\boldsymbol{x}}'$, with an associated initial estimation error covariance ($\mathbf{P}_{0,\boldsymbol{r}_r} = \mathbf{I}_{0,\boldsymbol{r}_r}^{-1}$) and $\mathbf{R} = \text{diag}[\sigma_{s_1}^2,\ \ldots,\ \sigma_{s_M}^2]$.

D. Optimal Transmitter Selection Problem

The optimal transmitter selection problem can be cast as the optimization problem

$$\begin{aligned}\underset{w}{\text{minimize}} \quad & \mathcal{J}(\boldsymbol{w})\\ \text{subject to} \quad & \mathbf{1}_M^{\mathsf{T}}\boldsymbol{w} = K\\ & w_i \in \{0,1\}, \quad i = 1,\ \ldots, M,\end{aligned}$$

where $\mathcal{J}(\boldsymbol{w})$ denotes a desired cost function (e.g., A-, D-, and E-optimality criterion or dilution of precision [44], [45]), w_i is a binary decision variable which determines whether to accept or reject the i^{th} measurement, $\boldsymbol{w} = [w_1,\ \ldots,\ w_M]^{\mathsf{T}}$ is a vector of the binary decision variables, $\mathbf{1}_M \in \mathbb{R}^M$ is a vector of ones, and K is the selection subset's cardinality. This optimization problem is computationally involved to solve in real-time due to the integer constraints. Instead of solving the above optimization problem, two efficient transmitter selection strategies are proposed in the next section.

IV. Transmitter Selection Framework

The proposed transmitter selection framework selects the most informative SOP subset to minimize the aerial vehicle's position error uncertainty. According to the simplification discussed in Subsection III-C, only the information contribution from the i^{th} SOP to the position states, denoted $\mathbf{I}_{\boldsymbol{r}_r,i}$, is used to evaluate the cost function $\mathcal{J}(\boldsymbol{w})$. Ergo, the cost function is defined as the A-optimality criterion: trace of the posterior position estimation error covariance (equivalently, trace of the inverse of FIM)

$$\begin{aligned}\mathcal{J}(\boldsymbol{w}) &\triangleq \text{tr}\left[\mathbf{I}_{0,\boldsymbol{r}_r} + \mathbf{H}_{\boldsymbol{r}_r}'^{\mathsf{T}}\text{diag}(\boldsymbol{w})\mathbf{H}_{\boldsymbol{r}_r}'\right]^{-1}\\ &= \text{tr}\left[\mathbf{I}_{0,\boldsymbol{r}_r} + \sum_{i=1}^{M} w_i\mathbf{I}_{\boldsymbol{r}_r,i}\right]^{-1}, \quad (5)\end{aligned}$$

where $\mathbf{H}_{\boldsymbol{r}_r}' \triangleq (\mathbf{R}_a^{-1})^{\mathsf{T}}\mathbf{H}_r$, $\mathbf{R}_a$ is the upper-triangular Cholesky factorized measurement covariance (i.e., $\mathbf{R} = \mathbf{R}_a^{\mathsf{T}}\mathbf{R}_a$), and $\mathbf{I}_{0,\boldsymbol{r}_r}$ is the prior FIM corresponding to the receiver's position states (see Fig. 3).

Algorithm 1 summarizes each of the proposed transmitter selection strategy's steps.

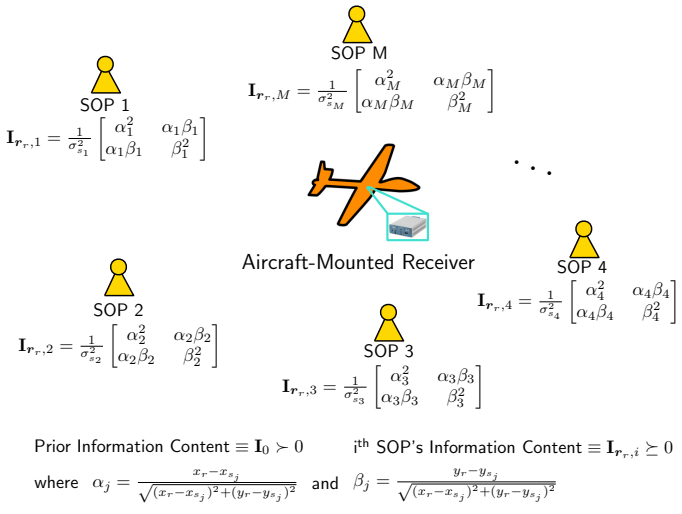

Fig. 3. Receiver estimating its two position states (i.e., $\hat{\boldsymbol{x}}' \in \mathbb{R}^2$) in an environment comprised of M terrestrial SOPs.

Algorithm 1 Transmitter Selection Strategies

Input: Prior FIM, FIM associated with each measurement, map of all SOPs, and number of SOPs to be selected
Output: SOP selection subset and FIM for the selected SOPs
1: Define an empty set for SOP selection
2: Perform an exhaustive search to select the two SOPs with the largest information content
3: Update the prior FIM and SOP selection subset
one-shot Selection (OSS)
4: Compute the posterior FIM for all SOPs, excluding those already selected
5: Choose the $K-2$ SOPs which minimize the receiver's average position error uncertainty
6: Compute the FIM for the selected SOPs (i.e., prior FIM plus all selected SOP's FIM) and update the SOP selection subset
7: **Return** SOP selection subset and FIM for the selected SOPs
Opportunistic Greedy Selection (OGS)
for $K-2$ **iterations**
4: Compute the posterior FIM for all SOPs, excluding those already selected
5: Choose one SOP which minimizes the receiver's average position error uncertainty
6: Redefine the prior FIM (i.e., (current) prior FIM plus selected SOP's FIM) and update the SOP selection subset
end for

V. Selection Strategy Analysis

This section will compare the selection subsets of the proposed transmitter selection strategies and provide an upper bound on the FIM for the selected range-only measurements.

A. OSS vs. OGS Selection Subset Comparison

The OSS and OGS will yield identical selection if the information content is scalar-valued, i.e., $x \in \mathbb{R}$ is constrained to one-dimension. This can be readily shown as follows. First, assume that the posterior FIM $I_{\text{posterior},i} = I_{0,r} + I_{\boldsymbol{r}_r,i}$ are ordered from smallest to largest, such that $\mathcal{J}\left(I_{\boldsymbol{w}^1}\right) \leq \mathcal{J}\left(I_{\boldsymbol{w}^2}\right) \leq \ldots \leq \mathcal{J}\left(I_{\boldsymbol{w}^K}\right) \leq \ldots \leq \mathcal{J}\left(\mathbf{I}_{\boldsymbol{w}^M}\right)$, where $\boldsymbol{w}^i$ is a vector of zeros with a one at the i^{th} element. Therefore, the OSS will yield the optimal selection set $S = \{1, 2, \ldots, K\}$, where the information content associated with the selected transmitters is denoted as $\mathbf{I} = \delta_0 + \frac{\xi_1}{\sigma^2_{s_1}} + \ldots + \frac{\xi_K}{\sigma^2_{s_K}}$. On the other hand, the OGS recursively selects one transmitter (i.e., $i = 1, \ldots, M$) which minimizes the cost function to yield

$$i^* = \underset{i}{\text{argmin}} \quad \left[\gamma_0 + \frac{\xi_3}{\sigma^2_{s_3}} + \frac{\xi_i}{\sigma^2_{s_i}}\right]^{-1}.$$

This selection process is performed at each iteration. By virtue of the simplifying assumption, the minimum argument (resulting in the smallest cost function) is selected in ascending order as $i^* = 4$, $i^* = 5, \ldots, i^* = K$ since $\mathcal{J}(\boldsymbol{w}^{i^*}) \leq \mathcal{J}(\boldsymbol{w}^i)$, $\forall i \setminus \{S\}$. Therefore, the transmitter selection subset will be $S = \{1, 2, \ldots, K\}$, where the information content associated with the selected transmitters is $I = \delta_0 + \frac{\xi_1}{\sigma^2_{s_1}} + \ldots + \frac{\xi_K}{\sigma^2_{s_K}}$, which is identical to the OSS.

For the 2-D case, i.e., $x \in \mathbb{R}^2$, the OSS and OGS will yield different selections. To show this, one proceeds similarly to the scalar case, noting that in the i^{th} iteration of the OGS

$$i^* = \underset{i \notin S}{\text{argmin}} \quad \text{tr}\left(\begin{bmatrix} \gamma'_{11} + \frac{\alpha_i^2}{\sigma^2_{s_i}} & \gamma'_{12} + \frac{\alpha_i\beta_i}{\sigma^2_{s_i}} \\ \gamma'_{12} + \frac{\alpha_i\beta_i}{\sigma^2_{s_i}} & \gamma'_{22} + \frac{\beta_i^2}{\sigma^2_{s_i}} \end{bmatrix}^{-1}\right).$$

This implies that the optimization problem's solution is heavily dependent on the cross-terms associated with the i^{th} SOP's posterior FIM. More specifically, each state's information content is coupled with one another. This affects the 2×2 FIM inverse via the determinant term which incorporates the mutually shared information shared (cross-terms) between the position state estimates. Therefore, $\mathcal{J}(\boldsymbol{w}^{i^*}) \not\leq \mathcal{J}(\boldsymbol{w}^i)$, $\forall i \setminus \{S\}$, yielding a different selection subset than the OSS.

B. Computational Complexity of OSS vs. OGS

If one attempts to find the optimal selection strategy by exhaustively searching, i.e., M choose K algorithm: $\binom{M}{K} = \frac{M!}{(M-K)!K!}$, the computational complexity is exponential, namely $O(M^K)$ for a large enough M, since $\binom{M}{K} = \frac{M^K}{K!}\left(1(1-\frac{1}{M})\cdots(1-\frac{K-1}{M})\right)$ where, K is assumed fixed and $1(1-\frac{1}{M})\cdots(1-\frac{K-1}{M}) \to 1$ as $M \to \infty$.

In contrast, the OGS computational complexity is $O(M^2) + O(K-2) \approx O(M^2)$, while the OSS computational complexity is $O(M^2) + O(1) \approx O(M^2)$, for a large enough M, both of which are quadratic. These can be derived by noting that the exhaustive search step's complexity is $\binom{M}{2} = \frac{M^2-M}{2!}$, where $\frac{1}{2!}(M^2 - M) \to M^2$ as $M \to \infty$. For OGS, the recursive search step's computational complexity is defined as $O(K-2)$ because it requires $K-2$ iterations to complete. For OSS, the batch selection step's computational complexity is defined as $O(1)$ because it only requires a single iteration to complete.

VI. Simulation Results

This section presents simulation results demonstrating the efficacy of the proposed OGS and OSS strategies, which are compared against the optimal selection, whose solution is obtained by exhaustive search $\binom{M}{K}$.

A. Optimal Selection, OSS, and OGS Strategy Comparison

The aerial vehicle is assumed to have initial access to GNSS signals, leading to knowledge of its initial position estimates $\hat{\boldsymbol{r}}_r(0)$, after which the aerial vehicle looses access to GNSS. During GNSS availability, the aerial vehicle chooses the "best" $K < M$ SOPs to use for navigation once GNSS signals are cut off.

The cellular SOP network was modeled as a binomial point process (BPP), where the horizontal positions of the SOPs are independently and uniformly distributed over an annular region centered at the aerial vehicle's current position O, i.e., $\mathbb{B}_O(d_{\min}, d_{\max}) = \pi(d_{\max}^2 - d_{\min}^2)$ [46], where $d_{\max}$ is the maximum distance for which ranging signals can be detected by the receiver and $d_{\min}$ is the minimum distance required for the far-field assumption to hold (see Fig. 4). The location of the i^{th} SOP with respect to the aerial vehicle can be parameterized in terms of the range R_i and bearing angle θ_i.

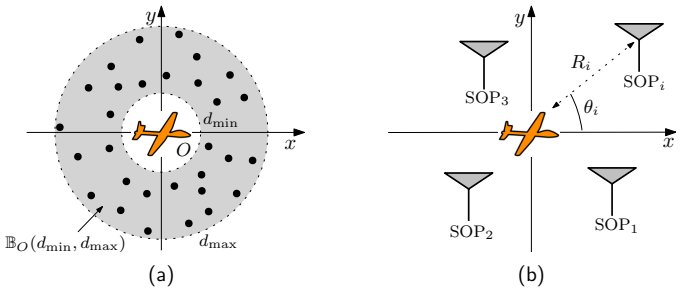

Fig. 4. (a) BPP realization with M = 22 SOPs. (b) Parameterization of the i^{th} SOP's position.

The simulation environment considered $M = 22$ terrestrial SOPs, of which $K \in \{6, 7, \ldots, 14\}$ are to be selected. For each K, 10^3 Monte Carlo (MC) realizations were generated according to the simulation settings summarized in Table I. The randomized MC realizations were the clock's process noise, measurement noise, and SOPs' locations. The three selection strategies (optimal, OSS, and OGS) were performed for each realization.

Fig. 5 compares the transmitter selection strategy performance for each K. The medium-sized green, blue, and red dots represent the cost function values for the optimal selection $\bar{\mathcal{J}}(\boldsymbol{w}_*)$, OGS $\bar{\mathcal{J}}(\boldsymbol{w}_{\text{OGS}})$, and OSS $\bar{\mathcal{J}}(\boldsymbol{w}_{\text{OSS}})$, respectively, *averaged* over all MC realizations. The tiny green, blue, and red dots represent the cost function value for each MC realization. It can be seen that, on one hand, the OGS yielded very close solution to the optimal value (the medium green and red dots are nearly on top of each other). The zoom below shows the difference between both solutions (i.e., $\bar{\mathcal{J}}(\boldsymbol{w}_*) - \bar{\mathcal{J}}(\boldsymbol{w}_{\text{OGS}})$). On the other hand, the OSS yielded solutions that were further than the optimal solution.

Table II shows the average cost function values $\bar{\mathcal{J}}(\boldsymbol{w})$ over all MC realizations along with the corresponding $\pm 1\sigma$. Note

TABLE I
Transmitter Selection Environment Simulation Settings

Parameter	Value
M	22
K	$\{6,\ 7,\ \ldots,\ 14\}$
$\boldsymbol{r}_r(0)$	$[0,\ 0]^{\mathsf{T}}$
$\mathbf{P}_{0,\boldsymbol{r}_r}$	$10^2 \cdot \mathbf{I}_{2\times 2}$
$\hat{\boldsymbol{r}}_r(0)$	$\sim \mathcal{N}\left[\boldsymbol{r}_r(0),\ \mathbf{P}_{\boldsymbol{r}_{0,\boldsymbol{r}_r}}\right]$
$\{R_i,\ \theta_i\}$	$\{\mathcal{U}[5,\ 80{,}000]$ m, $\mathcal{U}[-\pi,\ \pi]$ rad $\}$
$\boldsymbol{r}_{s_i}$	$[R_i\cos(\theta_i),\ R_i\sin(\theta_i)]^{\mathsf{T}}$
$\boldsymbol{x}_{\text{clk},i}(0)$	$c \cdot [9,\ 0.9]^{\mathsf{T}}$
$\{\boldsymbol{x}_{s_i}(0)\}_{i=1}^{M}$	$\left[\boldsymbol{r}_{s_i}^{\mathsf{T}}(0),\ \boldsymbol{x}_{\text{clk},i}^{\mathsf{T}}(0)\right]^{\mathsf{T}}$
$\{\mathbf{P}_{0,\text{clk},s_i}\}_{i=1}^{M}$	$\text{diag}[30\times 10^3,\ 0.3\times 10^3]$
$\{\hat{\boldsymbol{x}}_{\text{clk},s_i}(0)\}_{i=1}^{M}$	$\sim \mathcal{N}\left[\boldsymbol{x}_{\text{clk},i}(0),\ \mathbf{P}_{x_{0,\text{clk},s_i}}\right]$
$\{h_{0,\text{r}},\ h_{-2,\text{r}}\}$	$\{8.0\times 10^{-20},\ 4.0\times 10^{-23}\}$
$\{h_{0,s_i},\ h_{-2,s_i}\}_{i=1}^{M}$	$\{2.6\times 10^{-22},\ 4.0\times 10^{-26}\}$
$\{\sigma_{s_i}^2\}_{i=1}^{M}$	10 m^2
T	0.01 s

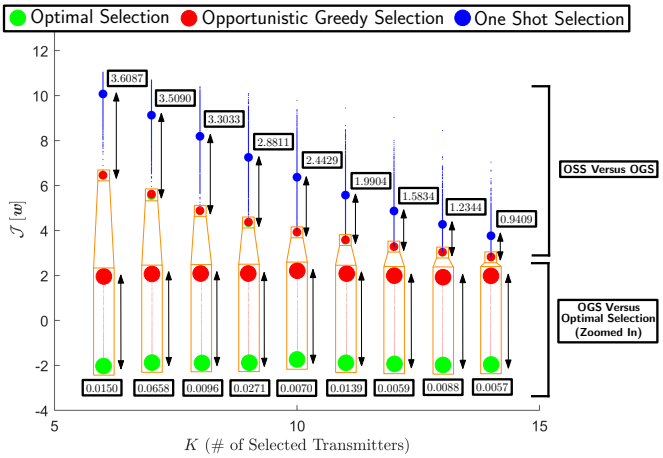

Fig. 5. Cost function point cloud with 10^3 MC realizations for optimal selection (green), OGS (red), and OSS (blue). The average cost function values over all MC realizations is shown as medium-sized dots, while the cost function value for each MC realization is represented as tiny dots. The top boxed values represent $\bar{\mathcal{J}}(\boldsymbol{w}_*) - \bar{\mathcal{J}}(\boldsymbol{w}_{\text{OSS}})$, while bottom boxed values (in the zoom in) represent $\bar{\mathcal{J}}(\boldsymbol{w}_*) - \bar{\mathcal{J}}(\boldsymbol{w}_{\text{OGS}})$.

that the average cost function values for the OGS and optimal selection strategies are very close to each other with a low standard deviation, whereas the OSS strategy is prone to worse selection performance (i.e., larger cost function value) with a higher standard deviation.

B. Effect of Timing on the Optimal Transmitter Selection

A simulation was conducted to justify the simplification invoked in Subsection III-C, whereby only the aerial vehicle's position states were considered, while ignoring the timing states. To this end, 250 MC realizations were generated, for each of which, the optimal transmitter selection strategy $\binom{M}{K}$ was performed to minimize (5) with the FIM

$$\mathbf{I}(\boldsymbol{x}') = \mathbf{I}_{0,\boldsymbol{r}_r}(\boldsymbol{x}') + \sum_{i=1}^{M} \frac{w_i}{\sigma_{s_i}^2} \begin{bmatrix} \alpha_i^2 & \alpha_i\beta_i \\ \alpha_i\beta_i & \beta_i^2 \end{bmatrix}.$$

TABLE II
AVERAGE COST FUNCTION VALUES FOR THE TRANSMITTER SELECTION STRATEGIES WITH $K = 6 - 14$

K	6	7	8	9	10	11	12	13	14
$\bar{\mathcal{J}}(\boldsymbol{w}_*)$ $[\pm\sigma_*]$	6.45 [±0.001]	5.56 [±0.005]	4.88 [±0.006]	4.35 [±0.009]	3.92 [±0.01]	3.57 [±0.01]	3.28 [±0.01]	3.03 [±0.02]	2.82 [±0.02]
$\bar{\mathcal{J}}(\boldsymbol{w}_{\text{OGS}})$ $[\pm\sigma_{\text{OGS}}]$	6.47 [±0.02]	5.62 [±0.02]	4.89 [±0.01]	4.38 [±0.01]	3.93 [±0.01]	3.59 [±0.02]	3.29 [±0.02]	3.04 [±0.02]	2.83 [±0.03]
$\bar{\mathcal{J}}(\boldsymbol{w}_{\text{OSS}})$ $[\pm\sigma_{\text{OSS}}]$	10.08 [±0.76]	9.13 [±0.99]	8.19 [±1.13]	7.26 [±1.19]	6.37 [±1.16]	5.58 [±1.08]	4.87 [±0.96]	4.28 [±0.84]	3.77 [±0.70]

TABLE III
REDUCTION IN AVERAGE POSITION UNCERTAINTY DUE TO OPTIMIZING THE FIM $\mathbf{I}(\boldsymbol{x})$ INSTEAD OF $\mathbf{I}(\boldsymbol{x}')$

K	6	7	8	9	10	11	12	13	14
Uncertainty reduction [m^2]	0.2630	0.2593	0.2643	0.2568	0.2862	0.2183	0.2781	0.2178	0.2475

Next, the FIM that considers the full state vector $\boldsymbol{x}$ (comprising position, velocity, and timing states) was used to find the optimal selection, i.e., minimize (5), but with the FIM

$$\mathbf{I}(\boldsymbol{x}) = \mathbf{I}_0(\boldsymbol{x}) + \begin{bmatrix} \sum_{i=1}^{M} \frac{w_i \alpha_i^2}{\sigma_{s_i}^2} & \sum_{i=1}^{M} \frac{w_i \alpha_i \beta_i}{\sigma_{s_i}^2} & \frac{w_1 \alpha_1}{\sigma_{s_1}^2} & \frac{w_2 \alpha_2}{\sigma_{s_2}^2} & \cdots & \frac{w_M \alpha_M}{\sigma_{s_M}^2} \\ \sum_{i=1}^{M} \frac{w_i \alpha_i \beta_i}{\sigma_{s_i}^2} & \sum_{i=1}^{M} \frac{w_i \beta_i^2}{\sigma_{s_i}^2} & \frac{w_1 \beta_1}{\sigma_{s_1}^2} & \frac{w_2 \beta_2}{\sigma_{s_2}^2} & \cdots & \frac{w_M \beta_M}{\sigma_{s_M}^2} \\ \frac{w_1 \alpha_1}{\sigma_{s_1}^2} & \frac{w_1 \beta_1}{\sigma_{s_1}^2} & \frac{w_1}{\sigma_{s_1}^2} & 0 & 0 & 0 \\ \frac{w_2 \alpha_2}{\sigma_{s_2}^2} & \frac{w_2 \beta_2}{\sigma_{s_2}^2} & 0 & \frac{w_2}{\sigma_{s_2}^2} & 0 & 0 \\ \vdots & \vdots & \vdots & \vdots & \ddots & \vdots \\ \frac{w_K \alpha_K}{\sigma_{s_K}^2} & \frac{w_K \beta_K}{\sigma_{s_K}^2} & 0 & 0 & 0 & \frac{w_K}{\sigma_{s_K}^2} \end{bmatrix}.$$

Table III tabulates the reduction in position uncertainty (averaged over all MC realizations for each K value) upon including the timing error states in the FIM. It can be noted that the reduction in position uncertainty is small (on the order of sub-meter), which justifies the considered simplification.

VII. EXPERIMENTAL RESULTS

This section demonstrates the efficacy of the proposed algorithms to select a "manageable" subset of terrestrial SOPs to navigate an aircraft in a real-world environment.

A. Hardware and Software Setup

The SNIFFER flight campaign took place on a Beechcraft C12 Huron (called Ms. Mabel), a fixed-wing U.S. Air Force aircraft, flown by members of the USAF Test Pilot School (TPS) over two different regions: (i) a rural region located in Edwards, California, USA, and (ii) a semi-urban region located in Palmdale, California, USA.

The C-12 aircraft was equipped with a quad-channel universal software radio peripheral (USRP)-2955, three consumer-grade 800/1900 MHz Laird cellular antennas, GPS antenna, a solid-state drive for data storage, PCIe cable, and a laptop computer running ASPIN Laboratory's software-defined radio (SDR), called MATRIX: Multichannel Adaptive TRansceiver Information eXtractor, for real-time monitoring of the cellular signals [27]. The MATRIX SDR produced the navigation observables: Doppler frequency, carrier phase, and pseudorange, along with the corresponding carrier-to-noise ratio (C/N_0). The experimental hardware setup is shown in Fig. 6.

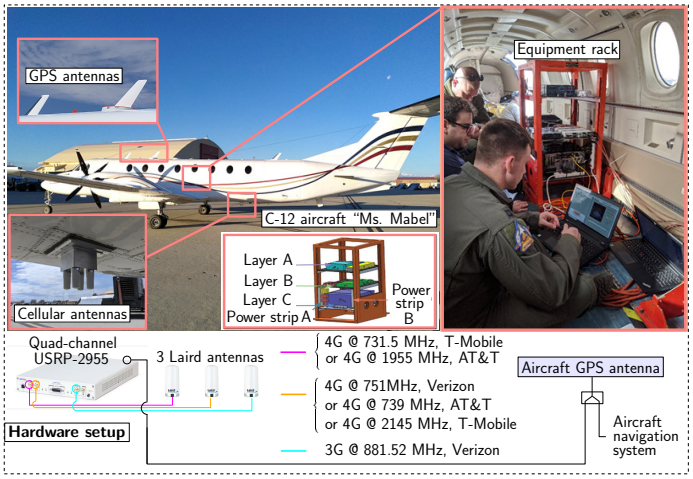

Fig. 6. Hardware setup equipped to the C-12 aircraft.

B. Transmitter Selection and Navigation Filter

The OGS and OSS selection strategies were performed in each of the two regions. To demonstrate the efficacy of the selected transmitters for aircraft navigation, the pseudorange measurements from the selected transmitters are fused with altimeter measurements via an extended Kalman filter (EKF), as described in [27]. The navigation solution was computed over a flight segment during which the selection strategies remained valid.

The EKF's initial state vector was set as $\hat{\boldsymbol{x}}(0) = [\hat{\boldsymbol{r}}_r(0)^\mathsf{T},\ \dot{\hat{\boldsymbol{r}}}_r(0)^\mathsf{T},\ c\hat{\dot{\delta}}t_1(0),\ c\hat{\dot{\delta}}t_1(0),\ \ldots,\ c\hat{\dot{\delta}}t_K(0), c\hat{\dot{\delta}}t_K(0)]^\mathsf{T}$ with a corresponding initial estimation error covariance $\mathbf{P}(0) = \text{diag}[10^2 \cdot \mathbf{I}_{3\times3},\ 10 \cdot \mathbf{I}_{3\times3},\ 10^8,\ 10, \ldots, 10^8,\ 10]$. The clock error states of each SOP was initialized using the pseudorange measurements from the initial two time epochs. Specifically, the clock bias was initialized as $c\hat{\delta}t_i(0) = z_{s_i}(0) - \|\boldsymbol{r}_r(0) - \boldsymbol{r}_{s_i}\|_2$ and the clock drift was initialized as $c\hat{\dot{\delta}}t_i(0) = \frac{1}{T}[z_{s_i}(1) - z_{s_i}(0) - \|\boldsymbol{r}_r(1) - \boldsymbol{r}_{s_i}\|_2 + \|\boldsymbol{r}_r(0) - \boldsymbol{r}_{s_i}\|_2]$.

The aircraft's dynamics was assumed to evolve according to the simple, yet effective, velocity random walk model [47], with power spectra of the continuous-time acceleration noise in the East (E), North (N), and Up (U) directions set as $\tilde{q}_E = \tilde{q}_N = 5$ m^2/s^3 and $\tilde{q}_U = 10^{-3}$ m^2/s^3, respectively.

The receiver's clock covariance $\mathbf{Q}_{\text{clk},r}$ was set to correspond to a low-quality temperature-compensated crystal oscillator (TCXO) with $h_{0,r} = 2.0 \times 10^{-19}$ s and $h_{-2,r} = 2.0 \times 10^{-20}$

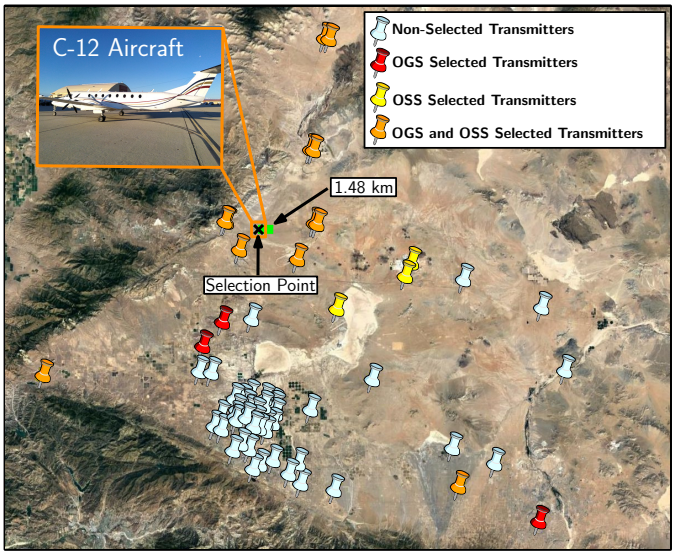

Fig. 7. Rural region transmitter selection results with OGS and OSS strategies during the aircraft's flight. Map data: Google Earth.

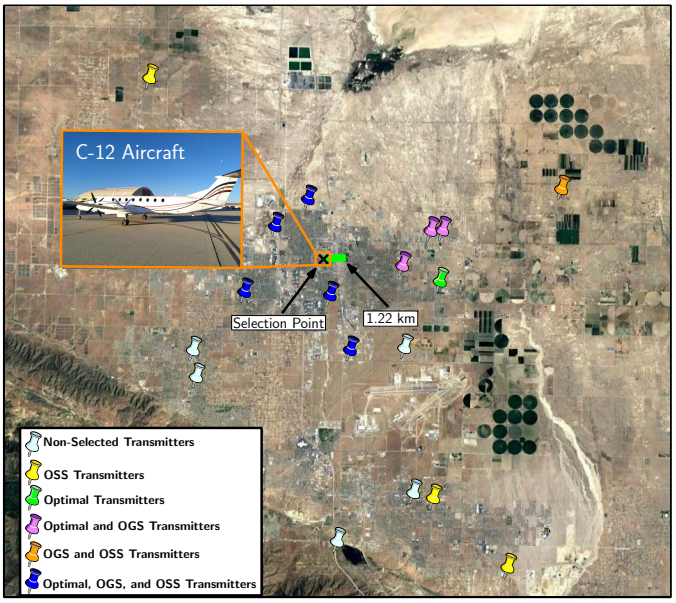

Fig. 8. Semi-urban region transmitter selection results with optimal selection, OGS, and OSS strategies during the aircraft's flight. Map Data: Google Earth.

s^{-1}. The SOPs' clock covariance $\mathbf{Q}_{\text{clk},s_i}$ was set to correspond to a typical-quality oven-controlled crystal oscillator (OCXO) with $h_{0,s_i} = 8.0 \times 10^{-20}$ s and $h_{-2,s_i} = 4.0 \times 10^{-23}$ s^{-1}. The time-varying measurement covariance $\mathbf{R}$ was proportional to the inverse of C/N_0 and the sampling time was $T = 0.01$ s.

C. Flight Region 1: Rural

The rural region was comprised of $M = 57$ terrestrial cellular SOPs, where the aircraft was tasked with selecting the most "informative" $K = 15$ SOPs to use for navigation.

Fig. 7 shows: (i) selected SOPs from OGS (red pins), (ii) selected SOPs from OSS (yellow pins), (iii) selected SOPs from both OSS and OGS strategies (orange pins), and (iv) and non-selected SOPs (white pins). Table VI compares the snapshot performance (A-, D-, and E-optimality and HDOP metrics) of the OGS versus OSS selection.

Upon selecting the SOPs, the aircraft navigated along the green trajectory in Fig. 7 for 1.48 km. It should be noted the optimal solution (i.e., global minimizer) for terrestrial SOP selection is infeasible to compute using the $\binom{M}{K}$ selection strategy due to its formidable run time. In light of this, 10^5 MC runs were performed in an attempt to capture a range of best-to-worst selections. Table IV summarizes the navigation performance when using the transmitters selected by the OGS, OSS, and MC realizations. It is worth noting that the OGS returned relatively comparable performance to the best-case MC realization. It is also worth noting the worst-case MC realization yielding much larger error than the best-case realization (i.e., the variance is rather large), which further motivates the importance of transmitter selection.

D. Flight Region 2: Semi-Urban

The semi-urban region was comprised of $M = 18$ terrestrial cellular SOPs, where the aircraft was tasked with selecting the most "informative" $K = 9$ SOPs to use for navigation.

The number of SOPs in this region was small enough to compute the optimal solution via the $\binom{M}{K}$ selection strategy to determine the global minimizer. Fig. 8 shows: (i) selected SOPs from $\binom{M}{K}$ (green pins), (ii) selected SOPs from OGS (violet pins), (iii) selected SOPs from OSS (yellow pins), (iii) selected SOPs from both OSS and OGS strategies (orange pins), (iv) selected SOPs from optimal, OSS, and OGS (blue pins), and (v) non-selected SOPs (white pins). Table VII compares the snapshot performance (A-, D-, and E-optimality and HDOP metrics) of the optimal versus OGS and OSS.

Upon selecting the SOPs, the aircraft navigated along the green trajectory in Fig. 8 for 1.22 km. Table V summarizes the navigation performance when using the transmitters selected by the optimal, OGS, and OSS. Note that the navigation performance with the OGS strategy is close to that of the optimal selection, whereas the OSS strategy performed slightly worse. This further motivates using the computationally efficient OGS selection strategy instead of the computationally expensive optimal selection strategy, over this valid selection region.

VIII. Conclusions

This article proposed computationally efficient transmitter selection strategies to select the most informative terrestrial SOPs to use when navigating an aerial vehicle. The strategies exploited the additive, iterative properties of the FIM to minimize the vehicle's average position error variance. Simulation results showed the OGS performance to be very close to the optimal selection, while executing in a fraction of the optimal selection's time. Experimental results in a real-world environment were presented showing the efficacy of the OGS and OSS strategies in navigating a U.S. Air Force high-altitude aircraft with terrestrial cellular SOPs. The achieved position RMSE with the optimal, OGS, and OSS solutions were 4.53 m, 6.28 m, 7.13 m in the rural region; and 5.83 m, 6.08 m, 6.70 m in the semi-urban region for an aircraft traversing a trajectory of 1.48 km and 1.22 km, respectively.

TABLE VI
EXPERIMENT 1: SNAPSHOT PERFORMANCE METRICS IN RURAL REGION AFTER TRANSMITTER SELECTION

Selection Type	$\mathrm{tr}[\mathbf{P}_{\boldsymbol{r}_r}]$	$\log[\det(\mathbf{P}_{\boldsymbol{r}_r})]$	$\lambda_{\max}[\mathbf{P}_{\mathbf{r}_r}]$	HDOP
OGS	200.99	9.20	100.00	0.54
OSS	200.99	9.20	100.00	0.54

TABLE VII
EXPERIMENT 2: SNAPSHOT PERFORMANCE METRICS IN SEMI-URBAN REGION AFTER TRANSMITTER SELECTION

Selection Type	$\mathrm{tr}[\mathbf{P}_{\boldsymbol{r}_r}]$	$\log[\det(\mathbf{P}_{\boldsymbol{r}_r})]$	$\lambda_{\max}[\mathbf{P}_{\mathbf{r}_r}]$	HDOP
Optimal Selection	200.99	9.20	100.00	0.74
OGS	200.99	9.20	100.00	0.88
OSS	200.99	9.20	100.00	0.94

APPENDIX A: CLOCK ERROR DYNAMICS

The aerial vehicle-mounted receiver's and SOP's clock error states are assumed to evolve according to

$$\boldsymbol{x}_{\mathrm{clk}}(k+1) = \mathbf{F}_{\mathrm{clk}}\,\boldsymbol{x}_{\mathrm{clk}}(k) + \boldsymbol{w}_{\mathrm{clk}}(k), \tag{6}$$
$$\boldsymbol{x}_{\mathrm{clk}} \triangleq \left[\, c\delta t,\, c\dot{\delta}t \,\right]^{\mathsf{T}}, \quad \mathbf{F}_{\mathrm{clk}} = \begin{bmatrix} 1 & T \\ 0 & 1 \end{bmatrix},$$

where δt is the clock bias, $\dot{\delta}t$ is the clock drift, c is the speed of light, T is the constant sampling interval, and $\boldsymbol{w}_{\mathrm{clk}}$ is the process noise, which is modeled as a discrete-time white noise sequence with covariance

$$\mathbf{Q}_{\mathrm{clk}} = c^2 \cdot \begin{bmatrix} S_{\tilde{w}_{\delta t}} T + S_{\tilde{w}_{\dot{\delta} t}} \frac{T^3}{3} & S_{\tilde{w}_{\dot{\delta} t}} \frac{T^2}{2} \\ S_{\tilde{w}_{\dot{\delta} t}} \frac{T^2}{2} & S_{\tilde{w}_{\dot{\delta} t}} T \end{bmatrix}. \tag{7}$$

The terms $S_{\tilde{w}_{\delta t}}$ and $S_{\tilde{w}_{\dot{\delta} t}}$ are the clock bias and drift process noise power spectral densities, respectively, which can be related to the power-law coefficients, $\{h_{\alpha_i}\}_{\alpha_i=-2}^{2}$, which have been shown through laboratory experiments to characterize the power spectral density (PSD) of the fractional frequency deviation of an oscillator from nominal frequency according to $S_{\tilde{w}_{\delta t}} \approx \frac{h_0}{2}$ and $S_{\tilde{w}_{\dot{\delta} t}} \approx 2\pi^2 h_{-2}$.

The receiver's and SOPs' process noise covariances $\mathbf{Q}_{\mathrm{clk},r}$ and $\{\mathbf{Q}_{\mathrm{clk},s_i}\}_{i=1}^{M}$ are calculated from (7) using the PSDs associated with the receiver's and SOPs' oscillator quality, respectively.

APPENDIX B: RELATIONSHIP BETWEEN WEIGHTED HDOP AND INFORMATION CONTENT

Dilution of precision (DOP) states how errors in the measurement will affect errors in the final estimates of the unknown quantities. The weighted horizontal dilution of precision (HDOP) matrix for the measurement vector $\boldsymbol{z}' \triangleq [z'_{s_1},\, \ldots,\, z'_{s_M}]^{\mathsf{T}}$ with an associated Jacobian matrix $\mathbf{H}$ defined in (3) and measurement covariance $\mathbf{R} = \mathrm{diag}[\sigma^2_{s_1}, \ldots, \sigma'^2_{s_M}]$, is defined as $\mathbf{D}_{\mathrm{w}} \triangleq [\mathbf{H}^{\mathsf{T}}\mathbf{R}^{-1}\mathbf{H}]^{-1}$, which has the form

$$\mathbf{D}_{\mathrm{w}} = \begin{bmatrix} \sigma_x^2 & \sigma_{xy}^2 \\ \sigma_{xy}^2 & \sigma_y^2 \end{bmatrix}, \tag{8}$$

The weighted HDOP is $\sqrt{\mathrm{tr}(\mathbf{D}_w)} = \sqrt{\sigma_x^2 + \sigma_y^2}$ [48].

The weighted HDOP matrix can be related to information content by the inverse of the estimation error covariance matrix as

$$\mathbf{D}_{\mathrm{w}}^{-1} = \sum_{j=1}^{K} \frac{1}{\sigma_{s_j}^2} \begin{bmatrix} \frac{(x_r - x_{s_j})^2}{(x_r-x_{s_j})^2+(yr-y_{s_j})^2} & \frac{(x_r-x_{s_j})(y_r-y_{s_j})}{(x_r-x_{s_j})^2+(yr-y_{s_j})^2} \\ \frac{(x_r-x_{s_j})(y_r-y_{s_j})}{(x_r-x_{s_j})^2+(yr-y_{s_j})^2} & \frac{(y_r-y_{s_j})^2}{(x_r-x_{s_j})^2+(yr-y_{s_j})^2} \end{bmatrix}$$
$$= \sum_{j=1}^{K} \frac{1}{\sigma_{s_j}^2} \begin{bmatrix} \alpha_j^2 & \alpha_j\beta_j \\ \alpha_j\beta_j & \beta_j^2 \end{bmatrix}$$

where α_j and β_j are variables which define the position unit vectors (i.e., $[\alpha_j,\ \beta_j]^{\mathsf{T}} = \frac{\boldsymbol{r}_r - \boldsymbol{r}_{s_j}}{\|\boldsymbol{r}_r - \boldsymbol{r}_{s_j}\|_2}$).

Additionally, the weighted HDOP matrix can be related to the information content in a closed form, defined by

$$\mathbf{D}_{\mathrm{w}} = \Lambda \sum_{j=1}^{K} \frac{1}{\sigma_{s_j}^2} \begin{bmatrix} \beta_j^2 & -\alpha_j\beta_j \\ -\alpha_j\beta_j & \alpha_j^2 \end{bmatrix}, \tag{9}$$

where

$$\Lambda = \left[\left\{ \sum_{j=1}^{K} \frac{\alpha_j^2}{\sigma_{s_j}^2} \right\} \left\{ \sum_{j=1}^{K} \frac{\beta_j^2}{\sigma_{s_j}^2} \right\} - \left\{ \sum_{j=1}^{K} \frac{\alpha_j\beta_j}{\sigma_{s_j}^2} \right\}^2 \right]^{-1}$$

TABLE IV
EXPERIMENT 1: NAVIGATION SOLUTION PERFORMANCE IN THE RURAL REGION

Selection Type	Pos. RMSE [m]	Vel. RMSE [m/s]	Max Pos. Error [m]	Max Vel. Error [m/s]	Run Time [ms]
10^5 MC Runs	[4.53, 71.55]	[0.98, 7.61]	[10.50, 125.06]	[5.90, 11.46]	–
OGS	6.28	1.44	10.50	6.38	19.30
OSS	7.13	1.39	10.50	6.38	16.50

TABLE V
EXPERIMENT 2: NAVIGATION SOLUTION PERFORMANCE IN THE SEMI-URBAN REGION

Selection Type	Pos. RMSE [m]	Vel. RMSE [m/s]	Max Pos. Error [m]	Max Vel. Error [m/s]	Run Time [ms]
Optimal Selection	5.84	1.45	10.80	5.90	700.30
OGS	6.08	1.42	10.80	5.90	5.30
OSS	6.70	1.35	10.80	5.90	3.90

is a constant value, corresponding to the information content of the position states, which is found in all HDOP terms. Finally, the HDOP constant can be defined as

$$\text{HDOP} = \sqrt{\Lambda \left\{ \sum_{j=1}^{K} \frac{1}{\sigma_{s_j}^2} \left(\beta_j^2 + \alpha_j^2 \right) \right\}} \tag{10}$$

ACKNOWLEDGMENTS

The authors would like to thank Ali Abdallah for his help with data processing as well as Tucker Haydon, Nadim Khairallah, and Mohammad Neinavaie for helpful discussions. The authors would like to thank Edwards Air Force Base (AFB) and Holloman AFB for inviting the ASPIN Laboratory to conduct experiments on U.S. Air Force aircraft in the "SNIFFER: Signals of opportunity for Navigation In Frequency-Forbidden EnviRonments" flight campaign. The authors would like to thank the U.S. Air Force pilots Chiawei Lee, Juan Jurado, Steven Wachtel, Jacob Duede, Zachary Hoeffner, Thomas Hulsey, and Rachel Quirarte and Republic of Singapore Air Force pilot RunXuan Tay. The authors would also like to thank Joe Khalife, Joshua Morales, Kimia Shamaei, Mahdi Maaref, Kyle Semelka, MyLinh Nguyen, and Trier Mortlock for their help with preparing for data collection. DISTRIBUTION STATEMENT A. Approved for public release; Distribution is unlimited. 412TW-PA-20146.

REFERENCES

[1] R. Sabatini, A. Roy, E. Blasch, K. Kramer, , G. Fasano, I. Majid, O. Crespillo, D. Brown, and R. Ogan, "Avionics systems panel research and innovation perspectives," *IEEE Aerospace and Electronic Systems Magazine*, vol. 35, no. 12, pp. 58–72, December 2020, doi: 10.1109/MAES.2020.3033475.

[2] EUROCONTROL, Aviation Intelligence Unit, "Does radio frequency interference to satellite navigation pose an increasing threat to network efficiency, cost-effectiveness and ultimately safety?" https://www.eurocontrol.int/sites/default/files/2021-03/eurocontrol-think-paper-9-radio-frequency-intereference-satellite-navigation.pdf, Tech. Rep., March 2021.

[3] International Civil Aviation Organization (ICAO), "An urgent need to address harmful interferences to GNSS," https://www.iata.org/contentassets/e45e5219cc8c4277a0e80562590793da/address-harmful-interferences-gnss.pdf, Tech. Rep., May 2019.

[4] J. Raquet *et al.*, "Position, navigation, and timing technologies in the 21st century," J. Morton, F. van Diggelen, J. Spilker, Jr., and B. Parkinson, Eds. Wiley-IEEE, 2021, vol. 2, Part D: Position, Navigation, and Timing Using Radio Signals-of-Opportunity, ch. 35–43, pp. 1115–1412, doi: 10.1002/9781119458555.ch35.

[5] J. Mortier, G. Pages, and J. Vila-Valls, "Robust TOA-based UAS navigation under model mismatch in GNSS-denied harsh environments," *Remote Sensing*, vol. 12, no. 18, pp. 2928–2947, September 2020.

[6] N. Souli, P. Kolios, and G. Ellinas, "Online relative positioning of autonomous vehicles using signals of opportunity," *IEEE Transactions on Intelligent Vehicles*, vol. 7, no. 4, pp. 873–885, 2022, doi: 10.1109/TIV.2021.3124727.

[7] Z. Kassas, J. Khalife, A. Abdallah, and C. Lee, "I am not afraid of the GPS jammer: resilient navigation via signals of opportunity in GPS-denied environments," *IEEE Aerospace and Electronic Systems Magazine*, vol. 37, no. 7, pp. 4–19, July 2022.

[8] M. Psiaki and B. Slosman, "Tracking of digital FM OFDM signals for the determination of navigation observables," in *Proceedings of ION GNSS Conference*, September 2019, pp. 2325–2348.

[9] X. Chen, Q. Wei, F. Wang, Z. Jun, S. Wu, and A. Men, "Super-resolution time of arrival estimation for a symbiotic FM radio data system," *IEEE Transactions on Broadcasting*, vol. 66, no. 4, pp. 847–856, December 2020.

[10] K. Shamaei and Z. Kassas, "Receiver design and time of arrival estimation for opportunistic localization with 5G signals," *IEEE Transactions on Wireless Communications*, vol. 20, no. 7, pp. 4716–4731, 2021, doi: 10.1109/TWC.2021.3061985.

[11] P. Wang, Y. Wang, and J. Morton, "Signal tracking algorithm with adaptive multipath mitigation and experimental results for LTE positioning receivers in urban environments," *IEEE Transactions on Aerospace and Electronic Systems*, vol. 58, no. 4, pp. 2779–2795, August 2022, 10.1109/TAES.2021.3139569.

[12] I. Lapin, G. Granados, J. Samson, O. Renaudin, F. Zanier, and L. Ries, "STARE: Real-time software receiver for LTE and 5G NR positioning and signal monitoring," in *Proceedings of Workshop on Satellite Navigation Technology*, April 2022, pp. 1–11, 10.1109/NAVITEC53682.2022.9847544.

[13] C. Yang, M. Arizabaleta-Diez, P. Weitkemper, and T. Pany, "An experimental analysis of cyclic and reference signals of 4G LTE for TOA estimation and positioning in mobile fading environments," *IEEE Aerospace and Electronic Systems Magazine*, vol. 37, no. 9, pp. 16–41, 2022, doi: 10.1109/MAES.2022.3186650.

[14] C. Yang and A. Soloviev, "Mobile positioning with signals of opportunity in urban and urban canyon environments," in *Proceedings of IEEE/ION Position, Location, and Navigation Symposium*, April 2020, pp. 1043–1059, doi: 10.1109/PLANS46316.2020.9109876.

[15] T. Hong, J. Sun, T. Jin, Y. Yi, and J. Qu, "Hybrid positioning with DTMB and LTE signals," in *Proceedings of International Wireless Communications and Mobile Computing*, July 2021, pp. 303–307, doi: 10.1109/IWCMC51323.2021.9498758.

[16] Z. Kassas, N. Khairallah, and S. Kozhaya, "Ad astra: Simultaneous tracking and navigation with megaconstellation LEO satellites," *IEEE Aerospace and Electronic Systems Magazine*, 2023, accepted.

[17] M. Hartnett, "Performance assessment of navigation using carrier Doppler measurements from multiple LEO constellations," Master's thesis, Air Force Institute of Technology, Ohio, USA, 2022.

[18] C. Huang, H. Qin, C. Zhao, and H. Liang, "Phase - time method: Accurate Doppler measurement for Iridium NEXT signals," *IEEE Transactions on Aerospace and Electronic Systems*, vol. 58, no. 6, pp. 5954–5962, 2022, 10.1109/TAES.2022.3180702.

[19] J. Khalife and Z. Kassas, "Opportunistic UAV navigation with carrier phase measurements from asynchronous cellular signals," *IEEE Transactions on Aerospace and Electronic Systems*, vol. 56, no. 4, pp. 3285–3301, August 2020, doi: 10.1109/TAES.2019.2948452.

[20] J. Khalife and Z. Kassas, "On the achievability of submeter-accurate UAV navigation with cellular signals exploiting loose network synchronization," *IEEE Transactions on Aerospace and Electronic Systems*, vol. 58, no. 5, pp. 4261–4278, October 2022, doi: 10.1109/TAES.2022.3162770.

[21] J. Khalife and Z. Kassas, "Differential framework for submeter-accurate vehicular navigation with cellular signals," *IEEE Transactions on Intelligent Vehicles*, vol. 8, no. 1, pp. 732–744, January 2023, doi: 10.1109/TAES.2022.3162770.

[22] N. Schneckenburger, T. Jost, D. Shutin, M. Walter, T. Thiasiriphet, M. Schnell, and U. Fiebig, "Measurement of the L-band air-to-ground channel for positioning applications," *IEEE Transactions on Aerospace and Electronic Systems*, vol. 52, no. 5, pp. 2281–2297, October 2016, doi: 10.1109/TAES.2016.150451.

[23] W. Khawaja, I. Guvenc, D. Matolak, U. Fiebig, and N. Schneckenburger, "A survey of air-to-ground propagation channel modeling for unmanned aerial vehicles," *IEEE Communications Surveys & Tutorials*, vol. 21, no. 3, pp. 2361–2391, 2019, doi: 10.1109/COMST.2019.2915069.

[24] E. Kim and Y. Shin, "Feasibility analysis of LTE-based UAS navigation in deep urban areas and DSRC augmentation," *Sensors*, vol. 19, no. 9, pp. 4192–4207, April 2019, doi: 10.3390/s19194192.

[25] B. Stevens and M. Younis, "Detection algorithm for cellular synchronization signals in airborne applications," *IEEE Access*, vol. 9, pp. 55 555–55 566, April 2021, doi: 10.1109/ACCESS.2021.3071674.

[26] Z. Kassas, A. Abdallah, J. Khalife, C. Lee, J. Jurado, J. Duede, Z. Hoeffner, T. Hulsey, R. Quirarte, S. Wachtel, and R. Tay, "Received power characterization of terrestrial cellular signals on high altitude aircraft," in *Proceedings of IEEE Aerospace Conference*, March 2022, pp. 1–8, doi: 10.1109/AERO53065.2022.9843492.

[27] Z. Kassas, J. Khalife, A. Abdallah, C. Lee, J. Jurado, S. Wachtel, J. Duede, Z. Hoeffner, T. Hulsey, R. Quirarte, and R. Tay, "Assessment of cellular signals of opportunity for high-altitude aircraft navigation," *IEEE Aerospace and Electronic Systems Magazine*, vol. 37, no. 10, pp. 4–19, October 2022, doi: 10.1109/MAES.2022.3187142.

[28] Z. Kassas, A. Abdallah, C. Lee, J. Jurado, J. Duede, Z. Hoeffner, T. Hulsey, R. Quirarte, S. Wachtel, and R. Tay, "Protecting the skies:

GNSS-less accurate aircraft navigation with terrestrial cellular signals of opportunity," in *Proceedings of ION GNSS Conference*, September 2022, pp. 1014–1025, doi: 10.33012/2022.18579.

[29] L. Kaplan, "Local node selection for localization in a distributed sensor network," *IEEE Transactions on Aerospace and Electronic Systems*, vol. 42, no. 1, pp. 136–146, March 2006, doi: 10.1109/TAES.2006.1603410.

[30] N. Cao, S. Choi, E. Masazade, and P. Varshney, "Sensor selection for target tracking in wireless sensor networks with uncertainty," *IEEE Transactions on Signal Processing*, vol. 64, no. 20, pp. 5191–5204, 2016, doi: 10.1109/TSP.2016.2595500.

[31] S. Joshi and S. Boyd, "Sensor selection via convex optimization," *IEEE Transactions on Signal Processing*, vol. 57, no. 2, pp. 451–462, February 2009, doi: 10.1109/TSP.2008.2007095.

[32] V. Kekatos and G. Giannakis, "Selecting reliable sensors via convex optimization," in *Proceedings of IEEE International Workshop on Signal Processing Advances in Wireless Communications*, June 2010, pp. 1–5.

[33] S. Liu, S. Chepuri, M. Fardad, E. Masazade, G. Leus, and P. Varshney, "Sensor selection for estimation with correlated measurement noise," *IEEE Transactions on Signal Processing*, vol. 64, no. 13, pp. 3509–3522, July 2016, doi: 10.1109/TSP.2016.2550005.

[34] Z. Dai, G. W. X. Jin, and X. Lou, "Nearly optimal sensor selection for TDOA-based source localization in wireless sensor networks," *IEEE Transactions on Vehicular Technology*, vol. 69, no. 10, pp. 12 031–12 042, July 2020, doi: 10.1109/TVT.2020.3011118.

[35] V. Cerone, S. Fosson, and D. Regruto, "A non-convex adaptive regularization approach to binary optimization," in *Proceedings of IEEE Conference on Decision and Control*, February 2021, pp. 3844–3849, doi: 10.1109/CDC45484.2021.9683667.

[36] A. Hashemi, M. Ghasemi, H. Vikalo, and U. Topcu, "Randomized greedy sensor selection: Leveraging weak submodularity," *IEEE Transactions on Automatic Control*, vol. 66, no. 1, pp. 199–212, January 2021, doi: 10.1109/TAC.2020.2980924.

[37] Y. Saito, T. Nonomura, K. Yamada, K. Nakai, T. Nagata, K. Asai, Y. Sasaki, and D. Tsubakino, "Determinant-based fast greedy sensor selection algorithm," *IEEE Access*, vol. 9, pp. 68 535–68 551, 2021, doi: 10.1109/ACCESS.2021.3076186.

[38] X. Shen and P. Varshney, "Sensor selection based on generalized information gain for target tracking in large sensor networks," *IEEE Transactions on Signal Processing*, vol. 62, no. 2, pp. 363–375, January 2014, doi: 10.1109/TSP.2013.2289881.

[39] F. Wang, X. Bai, B. Guo, and C. Liu, "Dynamic clustering in wireless sensor network for target tracking based on the Fisher information of modified Kalman filter," in *Proceedings of IEEE International Conference of Systems and Informatics*, November 2016, pp. 696–700, doi: 10.1109/ICSAI.2016.7811042.

[40] A. Nguyen and Z. Kassas, "Transmitter selection for improved information gathering in aerial vehicle navigation with terrestrial signals of opportunity," in *Proceedings of ION International Technical Meeting*, January 2022, pp. 723–734, doi: 10.33012/2022.18262.

[41] G. Mutambara, *Decentralized Estimation and Control for Multisensor Systems*. CRC Press, 1998.

[42] J. Morales, J. Khalife, and Z. Kassas, "Opportunity for accuracy," *GPS World Magazine*, vol. 27, no. 3, pp. 22–29, March 2016.

[43] M. Maaref, J. Khalife, and Z. Kassas, "Aerial vehicle protection level reduction by fusing GNSS and terrestrial signals of opportunity," *IEEE Transactions on Intelligent Transportation Systems*, vol. 22, no. 9, pp. 5976–5993, September 2021, doi: 10.1109/TITS.2021.3095184.

[44] D. Uciński, *Optimal Measurement Methods for Distributed Parameter System Identification*. CRC Press, 2005.

[45] N. Blanco-Delgado, F. Nunes, and G. Seco-Granados, "Relation between GDOP and the geometry of the satellite constellation," in *International Conference on Localization and GNSS*, June 2011, pp. 175–180, doi: 10.1109/ICL-GNSS.2011.5955282.

[46] S. Aditya, H. Dhillon, A. Molisch, R. Buehrer, and H. Behairy, "Characterizing the impact of SNR heterogeneity on time-of-arrival-based localization outage probability," *IEEE Transactions on Wireless Communications*, vol. 18, no. 1, pp. 637–649, January 2019, doi: 10.1109/TWC.2018.2883726.

[47] X. Li and V. Jilkov, "Survey of maneuvering target tracking. Part I: Dynamic models," *IEEE Transactions on Aerospace and Electronic Systems*, vol. 39, no. 4, pp. 1333–1364, 2003, doi: 10.1109/TAES.2003.1261132.

[48] D. Won, J. Ahn, S. Lee, J. Lee, S. Sung, H. Park, J. Park, and Y. Lee, "Weighted DOP with consideration on elevation-dependent range errors of GNSS satellites," *IEEE Transactions on Instrumentation and Measurement*, vol. 61, no. 12, pp. 3241–3250, December 2012, doi: 10.1109/TIM.2012.2205512.